Diaz-Rubio, Ana; Tretyakov, Sergei

Dual-Physics Metasurfaces for Simultaneous Manipulations of Acoustic and Electromagnetic Waves

Published in:
Physical Review Applied

DOI:
10.1103/PhysRevApplied.14.014076

Published: 24/07/2020

Document Version
Publisher's PDF, also known as Version of record

Please cite the original version:
Diaz-Rubio, A., & Tretyakov, S. (2020). Dual-Physics Metasurfaces for Simultaneous Manipulations of Acoustic and Electromagnetic Waves. *Physical Review Applied*, *14*(1), Article 014076. https://doi.org/10.1103/PhysRevApplied.14.014076

Dual-Physics Metasurfaces for Simultaneous Manipulations of Acoustic and Electromagnetic Waves

Ana Díaz-Rubio* and Sergei Tretyakov
Department of Electronics and Nanoengineering, Aalto University, P. O. Box 15500, Aalto FI-00076, Finland

(Received 22 February 2020; revised 11 March 2020; accepted 29 May 2020; published 24 July 2020)

In this work, we propose the use of power-flow–conformal metasurfaces for the creation of dual-physics devices that can simultaneously control waves of different natures. In particular, we introduce metasurface devices that perform specified operations on both electromagnetic and acoustic waves at the same time. Using a purely analytical model based on surface impedances, we introduce metasurfaces that perform the same functionality for electromagnetic and acoustic waves and, even more challenging, different functionalities for electromagnetics and acoustics. We provide realistic topologies for practical implementations of the proposed metasurfaces and confirm the results with numerical simulations.

DOI: 10.1103/PhysRevApplied.14.014076

I. INTRODUCTION

Over the past few years, great efforts have been concentrated on studying possibilities for controlling wave propagation using microstructured surfaces, so-called metasurfaces. Research on metasurfaces covers aspects from the theory of wave propagation, fabrication techniques, and even different disciplines or application fields such as acoustics [1] or electromagnetism [2,3]. Metasurfaces have shown great potential for manipulating waves both in transmission and reflection. In particular, metasurfaces controlling reflection, also known as metamirrors, have been developed for realizations of retroreflectors, anomalous reflectors, beam splitters, and focusing devices [4–13].

In the design of reflective metasurfaces, one can distinguish two different types of design strategy. On the one hand, there are examples of several *nonlocal design approaches*, where the properties on each point of the metasurface depend not only on the local field at the specific point but also on the fields in the vicinity of the point [5–7,10,11,14]. By exploiting nonlocality, it is possible to reduce the number of meta-atoms required for the implementation. However, the corresponding design approaches are complicated, especially for complex functionalities such as focusing. On the other hand, by using *local design approaches*, the properties of the metasurface at each point can be uniquely characterized by the response of the local fields at this point [8,12,13]. In this case, the metasurface can be characterized by local parameters such as the surface impedance. The main advantage of these methods is that with knowledge of the desired performance of the metasurface, the design of metasurfaces becomes systematic and in most of the cases it does not require numerical optimizations. In recent work [12], it has been demonstrated that the local design of metasurfaces is made possible by proper engineering of the shape and the surface impedance according to the power-flow distribution of the required set of waves.

In this work, we show that by exploiting the properties of local metasurfaces, one can design multiphysics devices that can simultaneously control waves of different natures. This becomes possible because power-flow–conformal metasurfaces can be realized as arrays of small (subwavelength) meta-atoms, which act as phase-shifting elements [12]. Here, we exploit the possibility of creating meta-atoms that can provide controllable phase shifts for both electromagnetic waves and for sound, which opens up a way toward the creation of high-performance multifunctional dual-physics metasurface devices.

Although acoustic and electromagnetic waves obey different wave-propagation equations that, respectively, govern sound-pressure and electromagnetic field distributions, there exists a direct analogy that allows us to create dual-physics structures [15]. In particular, we study the analogy of impedance-based models for electromagnetic and acoustic reflectors. In this paper, we exploit this analogy and present a direct and comparative approach for the design and implementation of power flow-conformal metamirrors for both acoustic and electromagnetic fields. We demonstrate that through the use of power-flow–conformal metamirrors and the local-parameter approach, the design of such devices becomes systematic and straightforward. Several example functionalities are analyzed and characterized in terms of the shape and surface impedance of the metamirror, as well as

*ana.diazrubio@aalto.fi

topologies of physical implementations. The study shows the similarities and differences between the two wave problems (acoustic and electromagnetic) that have to be considered in the final implementation of dual-physics platforms.

The paper is organized as follows. First, in Sec. II, we present the theory for the design of power-flow–conformal metasurfaces, paying special attention to the similarities and differences between the two domains of physics. In particular, the study focuses on the manipulation of two plane waves (retroreflectors and anomalous reflectors). This allows us to streamline the design of metasurfaces that allow simultaneous control of both acoustic and electromagnetic responses. Next, in Sec. III, we discuss practical aspects related to actual implementations of dual-physics metasurfaces. Finally, some conclusions summarize the main findings of this work.

II. GENERAL THEORETICAL FRAMEWORK

In this section, we present the theory of power-flow–conformal metasurfaces and highlight the differences between acoustic and electromagnetic devices for shaping reflected waves. More specifically, we discuss the design of reflective surfaces for reflecting an incident plane wave in a desired direction. The key parameter to be considered in the solutions of both problems is the surface impedance, which can be defined for both electromagnetic and acoustic waves (see, e.g., Refs. [16,17]).

Let us consider a curved impenetrable boundary lying on the x-z plane, the shape of which is defined by the function $y_c = f(x)$ (for simplicity, we assume that the surface profile is uniform along the orthogonal direction z). For acoustic waves, the surface impedance $Z_s(x)$ is defined as a relation between the pressure p and velocity $\mathbf{v}$ fields: $Z_s(x)\hat{\mathbf{n}} \cdot \mathbf{v}(x, y_c) = -p(x, y_c)$. Here, $\hat{\mathbf{n}}$ is the unit vector normal to the surface of the metamirror at point x. For electromagnetic waves, the surface impedance is defined as a relation between the tangential to the surface components of the electric and magnetic fields, $\mathbf{E}_t$ and $\mathbf{H}_t$, as $Z_s(x)\hat{\mathbf{n}} \times \mathbf{H}_t(x, y_c) = \mathbf{E}_t(x, y_c)$.

The wave fields above a perfect anomalously reflecting metasurface are sums of fields of only two plane waves: one is the incident plane wave and the other is the reflected plane wave, which propagates in the desired freely chosen direction. In order to find the optimal surface profile, $y_c = g(x)$, that ensures the desired functionalities of the metasurface, the first step is to analyze the distribution of power flow in this set of two plane waves [12]. In what follows, we analyze the power flow for both electromagnetic and acoustic problems.

Acoustic metamirror: The wave vectors of the waves can be defined as $\mathbf{k}_{i,r} = k_{i,r}^{(x)}\hat{\mathbf{x}} + k_{i,r}^{(y)}\hat{\mathbf{y}}$, where the subscript i (r) denotes the incident (reflected) plane wave. In the most general case, we can define the incident wave vector as $\mathbf{k}_i = k(\sin\theta_i\hat{\mathbf{x}} - \cos\theta_i\hat{\mathbf{y}})$, where θ_i is the incident angle (anticlockwise definition) and $k = \omega/c_{\text{ac}}$ is the wave number of sound waves in the background medium at the frequency of interest (c_{ac} is the speed of sound). Following the same notation, the wave vector of the reflected wave is defined as $\mathbf{k}_r = k(\sin\theta_r\hat{\mathbf{x}} + \cos\theta_r\hat{\mathbf{y}})$, where θ_r is the reflection angle (clockwise definition). A schematic representation of this scenario is shown in Fig. 1. Under the $e^{j\omega t}$ time convention, the field can expressed as follows:

$$p(x,y) = p_i e^{-j\mathbf{k}_i\cdot\mathbf{r}} + p_r e^{-j\mathbf{k}_r\cdot\mathbf{r}}, \tag{1}$$

$$v_x(x,y) = \frac{1}{\omega\rho}\left[p_i k_i^{(x)} e^{-j\mathbf{k}_i\cdot\mathbf{r}} + p_r k_r^{(x)} e^{-j\mathbf{k}_r\cdot\mathbf{r}}\right], \tag{2}$$

$$v_y(x,y) = \frac{1}{\omega\rho}\left[p_i k_i^{(y)} e^{-j\mathbf{k}_i\cdot\mathbf{r}} + p_r k_r^{(y)} e^{-j\mathbf{k}_r\cdot\mathbf{r}}\right], \tag{3}$$

where $p_i = |p_i|e^{j\phi_i}$ and $p_r = |p_r|e^{j\phi_r}$ are the complex amplitudes of the incident and reflected plane waves, $\mathbf{r} = x\hat{\mathbf{x}} + y\hat{\mathbf{y}}$ is the position vector, ω is the angular frequency, and ρ is the density of the background media. From the definition of the pressure and velocity vector, it is straightforward to derive the intensity vector of the superposition of both incident and reflected plane waves as $\mathbf{I}(x,y) = \frac{1}{2}\text{Re}(p\mathbf{v}^*) = I_x(x,y)\hat{\mathbf{x}} + I_y(x,y)\hat{\mathbf{y}}$. The analytical expression for the flow of power carried by two arbitrary plane waves reads

$$I_x(x,y) = \frac{1}{2\omega\rho}\left[|p_i|^2 k_i^{(x)} + |p_r|^2 k_r^{(x)}\right] + \frac{1}{2\omega\rho}|p_i||p_r|(k_i^{(x)} + k_r^{(x)})\cos(\Delta\mathbf{k}\cdot\mathbf{r} + \Delta\phi) \tag{4}$$

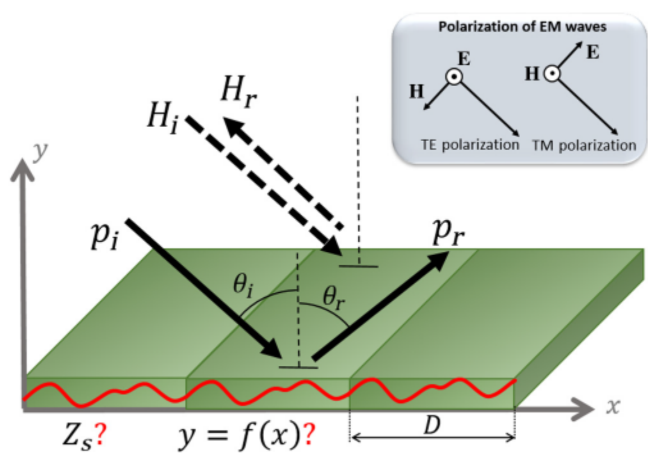

FIG. 1. A schematic representation of a dual-physics metasurface.

and

$$I_y(x,y) = \frac{1}{2\omega\rho}\left[|p_i|^2 k_i^{(y)} + |p_r|^2 k_r^{(y)}\right] + \frac{1}{2\omega\rho}\left[|p_i||p_r|(k_i^{(y)} + k_r^{(y)})\cos(\Delta\mathbf{k}\cdot\mathbf{r} + \Delta\phi)\right], \quad (5)$$

where $\Delta\mathbf{k} = \mathbf{k}_r - \mathbf{k}_i$ and $\Delta\phi = \phi_i - \phi_r$.

Electromagnetic metamirror: The analysis of the power-flow distribution for electromagnetic waves can be done following a similar approach. Because of the vectorial nature of the problem, here we should distinguish between TM-polarized (H_z, E_x, and E_y) and TE-polarized (E_z, H_x, and H_y) waves. Note that in this work we do not consider any change in the polarization state and we assume that both incident and reflected waves have the same polarization. As has been shown in Ref. [12], the power-flow distribution in the electromagnetic counterpart, defined by the Poynting vector $\mathbf{S} = \frac{1}{2}\mathrm{Re}(\mathbf{E}\times\mathbf{H}^*) = S_x(x,y)\hat{\mathbf{x}} + S_y(x,y)\hat{\mathbf{y}}$, is given by similar expressions as in Eqs. (4) and (5). There is a clear analogy between the two physical problems: For TM-polarized waves, the amplitude of the pressure fields is analogous to the amplitude of the magnetic fields ($p_{i,r} \rightarrow H_{i,r}$) and the density of the background media to the permittivity ($\rho \rightarrow \varepsilon_0$). For TE-polarized waves, the amplitude of electric fields plays the role of the amplitude of the pressure fields ($p_{i,r} \rightarrow E_{i,r}$) and the density of the background media is analogous to the permeability ($\rho \rightarrow \mu_0$).

From the analysis of the power-flow density distribution, we can see that the power-flow distribution mainly depends on the amplitude of the plane waves ($|p_i|$ and ($|p_r|$) and the direction of propagation ($\mathbf{k}_i$ and $\mathbf{k}_r$). We can distinguish three different scenarios depending on the relations between these parameters. (i) When $|p_i| = |p_r|$ and $\mathbf{k}_r = -\mathbf{k}_i$, the wave is reflected back toward the source; we call this the retroreflection scenario. (ii) Reflections with $|p_i| = |p_r|$ but $\mathbf{k}_r \neq \mathbf{k}_i$ can be realized if the wave reflects specularly. (iii) Finally, full power reflection is possible with $|p_i| \neq |p_r|$ and $\mathbf{k}_r \neq \mathbf{k}_i$; this case is usually called anomalous reflection. In the following, we consider in detail realizations of all these scenarios.

A. Retroreflection

The first case under study is the retroreflection scenario, i.e., we study surfaces capable of redirecting all the energy of an incident plane wave into the opposite direction ($\mathbf{k}_r = -\mathbf{k}_i$), back to the source. First, we analyze acoustic retroreflectors. In order to ensure power conservation, the amplitudes of the incident and reflected waves should be equal: $|p_i| = |p_r|$. By substituting these values in Eqs. (4) and (5), we can see that the intensity power-flow vector is zero at all points of space, $I_x(x,y) = I_y(x,y) = 0$. This means that in this special case we can design local retroreflectors with any shape, as the power will never cross the reflector boundary.

Figure 2 shows three different retroreflectors designed for $\theta_i = 70°$. The first example corresponds to a flat retroreflector, where the surface profile is defined as $y_c = 0$. Figure 2(b) shows the required normalized surface impedance. In the acoustic case, the impedance is normalized with respect to $Z_0 = Z_0^{\mathrm{ac}} = c_{\mathrm{ac}}\rho$. The surface-impedance function defines the period of the reflector and reads $D = \lambda/(2\sin\theta_i)$. The results of numerical simulations of the reflected pressure field are shown in Fig. 2(a), where we can see the reflected plane wave propagating in the opposite direction with respect to that of the incident plane wave. The second example is a retroreflector with a cosine surface profile $y_c = (\lambda/5)\cos(2\pi x/D)$ with the same period as the flat reflector. Figures 2(c) and 2(d) show the reflected field and the normalized surface impedance for this design. We can see that the surface impedance is also purely imaginary, confirming the local nature of the design.

The last example is a retroreflector with a cosine modulation, where the period is double of that for the flat reflector: $D' = 2D$. The curve that describes this surface-modulation profile can be expressed as $y_c = (\lambda/5)\cos(\pi x/D)$. The reflected field and the corresponding surface impedance are shown in Figs. 2(e) and 2(f). It is important to mention that the spatial periodicity of the metasurface can be used as a control parameter for the diffracted modes in the system, allowing us to control reflection for illuminations from other directions.

For the design of electromagnetic retroreflectors, even though the physical meaning of the surface impedance is different, we can use the mathematical analogy with the acoustic scenario. The correspondence between the normalized acoustic and electromagnetic impedances for TE-polarized waves is direct: $Z_s^{\mathrm{ac}}/Z_0^{\mathrm{ac}} = Z_s^{\mathrm{TE}}/Z_0^{\mathrm{EM}}$, where $Z_0^{\mathrm{ac}} = c_{\mathrm{ac}}\rho$ is the acoustic wave impedance and $Z_0^{\mathrm{EM}} = c_{\mathrm{EM}}\mu$ is the electromagnetic wave impedance. Here, c_{ac} and c_{EM} are the speed of sound and light, respectively. ρ is the mechanical density of the medium. However, for TM-polarized waves we obtain, due to the duality of the problem, that $Z_s^{\mathrm{ac}}/Z_0^{\mathrm{ac}} = Z_0^{\mathrm{EM}}/Z_s^{\mathrm{TM}} = Z_0^{\mathrm{EM}}Y_s^{\mathrm{TM}}$. As we show, these relations between required surface impedances will define certain constraints in the design of dual-physics metasurfaces.

B. Specular reflection

Next, we consider reflection into a wave with the same amplitude, $|p_i| = |p_r|$, but propagating in another direction, with $\mathbf{k}_r \neq \mathbf{k}_i$. In this case, from Eqs. (4) and (5), we can see that, in general, $I_x(x,y) \neq 0$ and $I_y(x,y) \neq 0$. As an example, Fig. 3(a) shows the power-flow distribution in two interfering plane waves when $\theta_i = 0°$ and $\theta_r = 70°$. It is

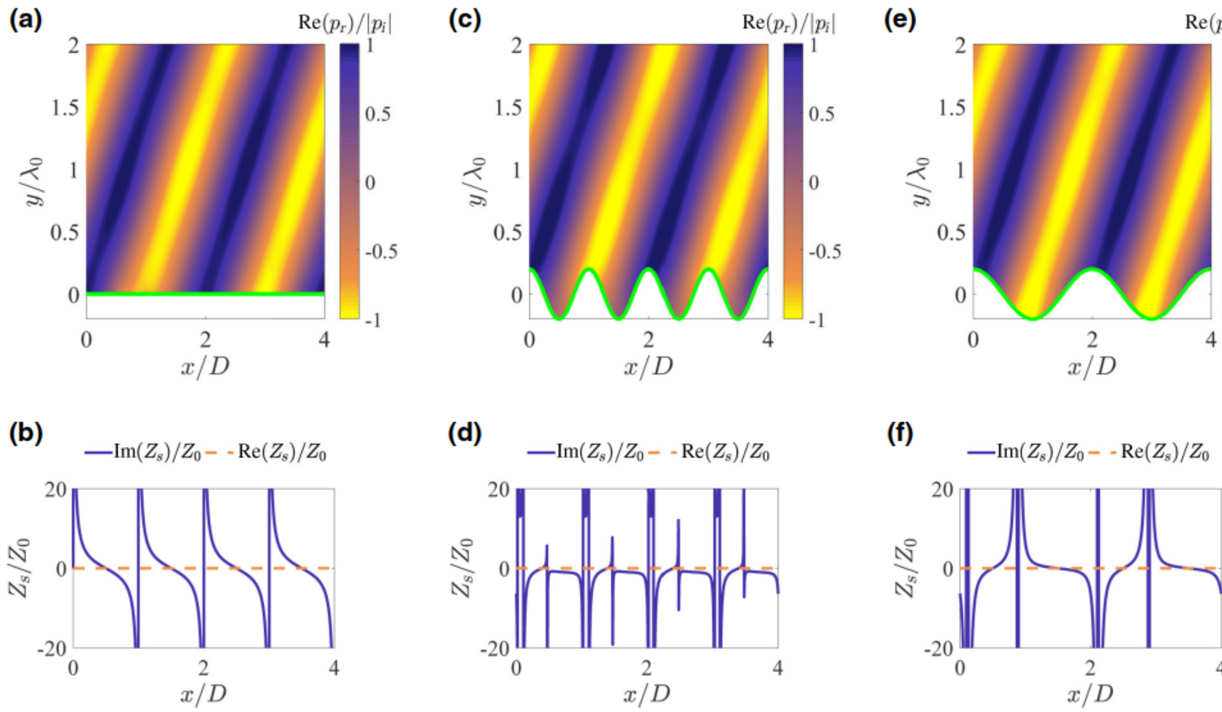

FIG. 2. Acoustic power-flow–conformal retroreflectors for $\theta_i = 70°$. (a),(b) The reflected pressure field (a) and the normalized surface impedance (b) for the flat retroreflector. (c),(d) The reflected pressure field (c) and the normalized surface impedance (d) for the retroreflector with cosine profile $y_c = (\lambda/5)\cos(2\pi x/D)$. (e),(f) The reflected pressure field (e) and the normalized surface impedance (f) for the retroreflector with cosine profile $y_c = (\lambda/5)\cos(\pi x/D)$.

clear from the analysis of the power flow that the surfaces through which there is no power flow are flat surfaces. Figure 3(b) shows a set of surfaces that are tangential to the intensity vector. The inclination angle can be written as $\theta_s = \arctan[(\sin\theta_i + \sin\theta_r)/(-\cos\theta_i + \cos\theta_r)]$. The components of the unit normal vector $\mathbf{n} = n_x\hat{\mathbf{x}} + n_y\hat{\mathbf{y}}$ are defined as $n_x = \frac{1}{\sqrt{2}}(\sin\theta_i + \sin\theta_r)$ and $n_y = \frac{1}{\sqrt{2}}(\cos\theta_i - \cos\theta_r)$. Clearly, these results correspond to trivial specular reflection from these flat surfaces.

The required impedances for each surface are represented in Fig. 3(c). We see that the surface impedances are purely imaginary and constant along the surfaces. Depending on the defined surface, the surface impedance takes different values to ensure the desired phase shift between the incident and reflected waves. We can find positions of surfaces acting as perfect electric conductors (PECs), where $Z_s = 0$, which corresponds to surfaces at the planes of zero intensity vector. On the contrary, surfaces with the behavior of a perfect magnetic conductor (PMC), characterized by $Z_s = \infty$, are located at the planes of the maximum intensity vector.

C. Anomalous reflection

The third and most interesting and general case is lossless reflection of a plane wave in an arbitrary direction, where in general both the amplitudes and the propagation directions are different: $|p_i| \neq |p_r|$, $(\mathbf{k}_r \neq \mathbf{k}_i)$. This scenario is known as anomalous reflection. For flat metasurfaces lying in the x-z plane, it is demonstrated that the relation between the incident and the reflected amplitudes is given by $R = |p_r|/|p_i| = \sqrt{\cos\theta_i/\cos\theta_r}$. The power-flow distribution for the case of $\theta_i = 0°$ and $\theta_r = 80°$ is shown in Fig. 4(a).

As has been proposed in Ref. [12], instead of trying to synthesize flat surfaces with the required complex-valued impedances, we can create the desired field distribution by shaping an impenetrable lossless reflector along surfaces that are tangential to the intensity vector. These surfaces can be found using the scalar function

$$g(x,y) = Ay + B\sin(\Delta\mathbf{k}\cdot\mathbf{r} + \Delta\phi) + C, \tag{6}$$

where $A = (1/2\omega\rho)|p_i|^2 k_0(\sin\theta_i + \cos\theta_i\tan\theta_r)$, $B = (1/2\omega\rho)|p_i|\sqrt{\cos\theta_i/\cos\theta_r}(\cos\theta_i - \cos\theta_r)/(\sin\theta_r - \sin\theta_i)$, and C is an arbitrary constant. This scalar function satisfies $\nabla g(x,y) = \mathbf{N}(x,y)$, with vector $\mathbf{N}(x,y) = -I_y(x,y)\hat{\mathbf{x}} + I_x(x,y)\hat{\mathbf{y}}$ being orthogonal to the intensity vector. From the properties of the gradient, the surfaces tangential to the power-flow directions can be calculated as the level curves of the function $g(x,y)$ and can be expressed as $y_c = f(x)$. Figure 4(b) shows different surface profiles for anomalous reflectors when $\theta_i = 0°$ and $\theta_r = 80°$.

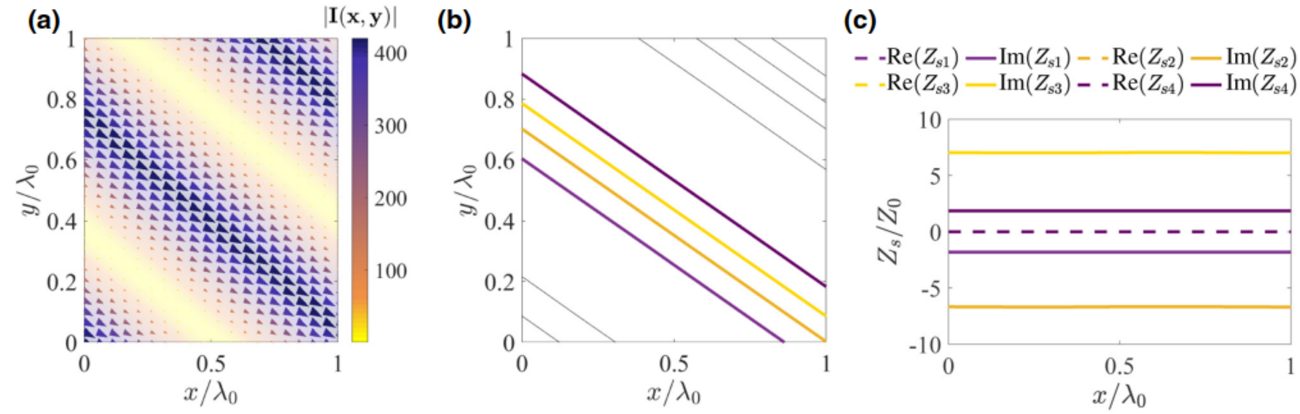

FIG. 3. The results for sets of two plane waves with $|p_i| = |p_r|$, $\theta_i = 0°$, and $\theta_r = 70°$: (a) the power-flow distribution; (b) the set of surfaces tangential to the intensity vector; and (c) the corresponding surface impedance associated with each surface. The four surfaces are denoted by subscripts 1, 2, 3, and 4.

Probably the most studied case in the literature of anomalous reflection is a normally incident plane wave ($\theta_i = 0$) that is redirected in an arbitrary direction ($\theta_r \neq 0$). In this case, the surface profile and the surface impedance are different for each specific angle of reflection. Figure 4(d) shows the shapes of the perfectly anomalously

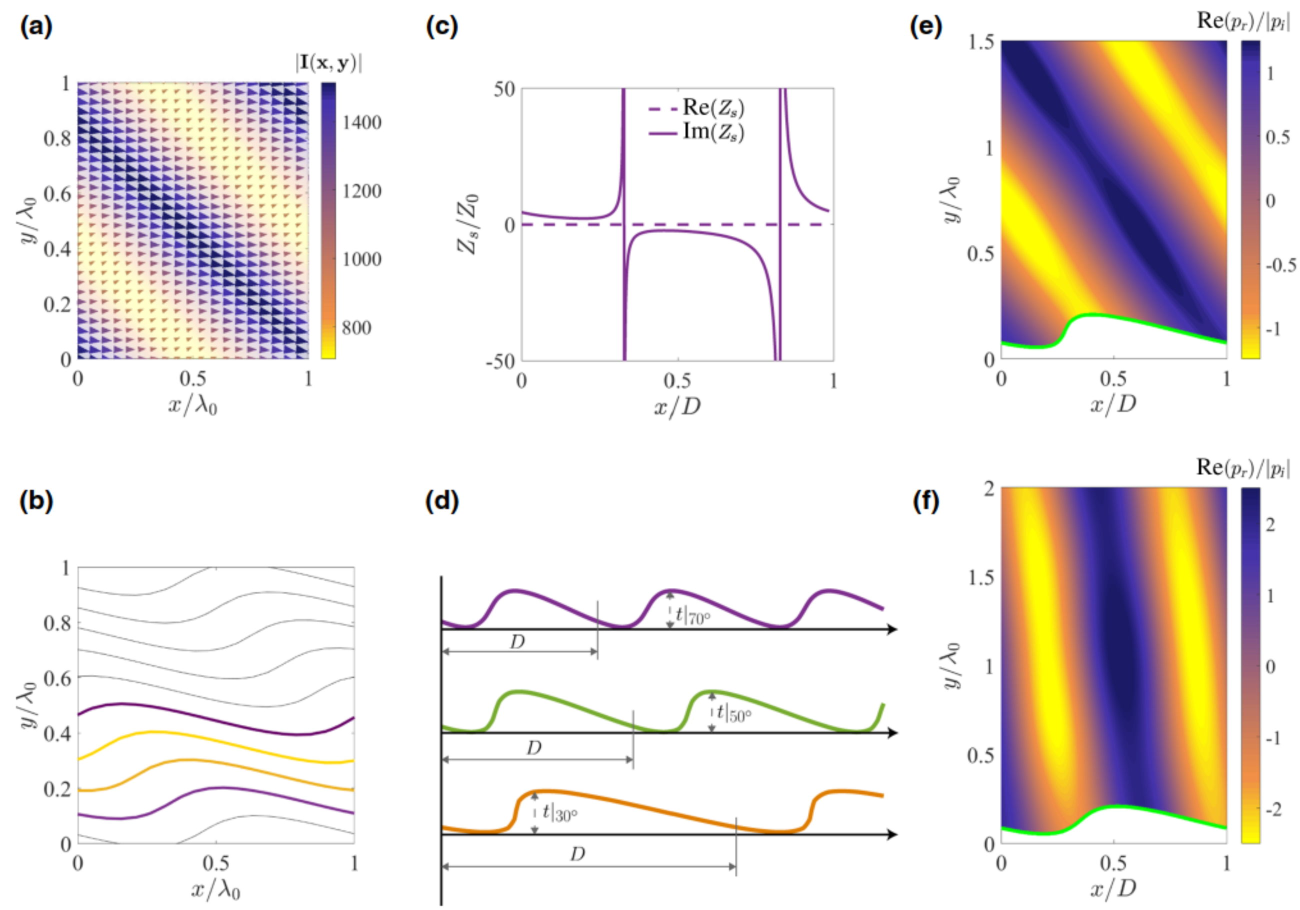

FIG. 4. The power-flow–conformal metamirror for acoustic anomalous reflectors. (a) The power-flow distribution for $\theta_i = 0°$ and $\theta_r = 80°$. (b) Surface profiles for anomalous reflection when $\theta_r = 80°$. (c) The surface impedance when $\theta_i = 0°$ and $\theta_r = 80°$. (d) Surface profiles for $\theta_i = 0°$ and $\theta_r = 30°$, $50°$, and $70°$. (e),(f) Numerical simulations for $\theta_i = 0°$ and $\theta_r = 80°$ and $\theta_i = 0°$ and $\theta_r = 70°$.

reflecting surfaces for $\theta_r = 30°, 50°$, and $70°$. As can be expected, the period of the surface modulation changes with the reflected angle according to $D = \lambda/(\sin\theta_r - \sin\theta_i)$. The amplitude of the modulation, h, stays almost constant for different incident angles ($h|_{30°} = 0.1566\lambda$, $h|_{50°} = 0.1538\lambda$, and $h|_{70°} = 0.1386\lambda$) and is always subwavelength. The required surface impedances for these particular surfaces are plotted in Fig. 4(c), for $\theta_r = 70°$. Two numerically simulated examples are presented in Figs. 4(e) and 4(f).

III. DUAL-PHYSICS IMPLEMENTATION

Here, we show that using the concept of power-flow–conformal metamirrors and the analogy between acoustic and electromagnetic impedances, it is possible to create metasurfaces that operate as retro- and most general anomalous reflectors simultaneously for both acoustic and electromagnetic waves.

As explained above, the metasurface functionalities are defined by the surface profile and the surface impedance. First, if we want to control both acoustic and electromagnetic waves, we need to ensure that the surface profiles required for both operations are compatible. As mentioned in the previous section, some scenarios, such as anomalous reflection, require specific surface profiles. However, in other cases there is no such restriction and one can use different surface profiles for the same functionality, such as for realizing retroreflectors. With this in mind, we distinguish two different design approaches: (i) platforms that implement the same functionality for acoustic and electromagnetic waves and (ii) platforms with different functionalities for acoustic and electromagnetic waves.

The second consideration is the design of the meta-atoms for implementing the corresponding surface impedance. Power-flow–conformal metasurfaces are described by locally defined acoustic or electromagnetic surface impedances, which allows implementations using conventional phase shifters of different types. The main challenge in the multiphysics realizations is to find such meta-atom configurations that will provide the desired phase shifts both for sound and electromagnetic waves. We identify three different structures that can be used for achieving this goal. The choice between them is made based on specific conditions in each design. The schematic representations of the proposed three topologies are shown in Fig. 5.

The first meta-atom is a closed-ended groove [see Fig. 5(a)]. Since here we consider surfaces that are modulated only along one direction, we assume that the grooves are infinitely long and uniform. If the thickness of the walls is much smaller than the width of the grooves, we can neglect the effect of wall thickness on the surface impedance. The acoustic surface impedance $Z_s^{\text{ac}} = -jZ_0^{\text{ac}}\cot(k_{\text{ac}}\ell)$ is controlled by the depth of the grooves ℓ and the acoustic impedance $Z_0^{\text{ac}} = c_{\text{ac}}\rho$ of the air filling the tube. Here, $k_{\text{ac}} = 2\pi f_{\text{ac}}/c_{\text{ac}}$ is the acoustic wave number. For TE-polarized electromagnetic waves (electric field parallel to the groove), in the microwave range an array of grooves reflects as a practically perfectly conducting surface (i.e., PEC) if the walls are made of metal and the width of the grooves is deeply subwavelength. For TM-polarized electromagnetic waves, the response of the meta-atom is defined by the surface impedance $Z_s^{\text{EM}} = jZ_0^{\text{EM}}\tan(k_{\text{EM}}\ell)$, where $Z_0^{\text{EM}} = \sqrt{\mu_0/\varepsilon_0}$ and $k_{\text{EM}} = 2\pi f_{\text{EM}}/c_{\text{EM}}$ are the electromagnetic wave impedance and the wave number in air, respectively.

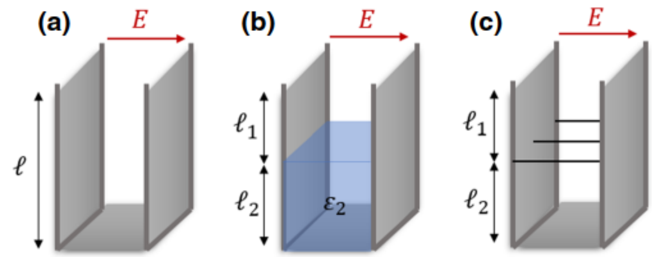

FIG. 5. Dual-physics meta-atoms: (a) empty closed-ended grooves; (b) partially filled closed-ended grooves; (c) closed-ended grooves with a metallic grid.

The second proposed topology is the same closed-ended groove but partially filled with a dielectric material with permittivity ε_2. The dielectric material should be chosen to behave as a hard boundary for acoustic waves, introducing strong impedance contrast with air for acoustic waves. In practice, one can consider solid plastics or water. As we can see in Fig. 5(b), the filling with length ℓ_2 is placed at the bottom of the groove. The length of the air layer is denoted as ℓ_1. The acoustic response of this meta-atom is defined by $Z_s^{\text{ac}} = -jZ_0^{\text{ac}}\cot(k_{\text{ac}}\ell_1)$. In contrast, the electromagnetic response for TM-polarized waves is given by the following surface impedance:

$$Z_s^{\text{EM}} = jZ_0^{\text{EM}}\frac{\tan(k_{\text{EM}}^{(2)}\ell_2) + \tan(k_{\text{EM}}\ell_1)}{1 - \tan(k_{\text{EM}}^{(2)}\ell_2)\tan(k_{\text{EM}}\ell_1)}. \tag{7}$$

Thus, the use of this structure allows us to independently tune both acoustic and electromagnetic impedances to the required values.

The third proposed topology is shown in Fig. 5(c). In this case, we use a groove of total depth $\ell = \ell_1 + \ell_2$ with an array of metal wires oriented in the same direction as the electric field of TM-polarized waves and positioned at distance ℓ_2 from the bottom of the groove. The array of metal wires has a period d_w small enough for the array to act as a nearly perfect electric wall for electromagnetic waves. The reflection of electromagnetic waves is very strong when the period of the array of wires is much smaller than the wavelength of the electromagnetic waves, while the diameter of the wires is still very small compared with the period [18]. This property allows us to realize a wire array that is a nearly perfect reflector for electromagnetic waves and that is nearly perfectly transparent for sound. The electromagnetic response of this meta-atom is characterized by the surface impedance $Z_s^{\rm EM} = jZ_0^{\rm EM}\tan(k_{\rm EM}\ell_1)$, while the acoustic response is defined by $Z_s^{\rm ac} = -jZ_0^{\rm ac}\cot(k_{\rm ac}\ell)$. Again, we see that there is a possibility of adjusting both impedances independently.

Using these meta-atoms, we can systematically design various devices for simultaneous control of electromagnetic and acoustic waves.

A. The same functionality in one platform

Here, we explore the possibilities of implementing metasurfaces with the same functionality for both electromagnetic and acoustic waves. In particular, we use the proposed meta-atoms to implement dual-physics retroreflectors and anomalous reflectors.

1. Dual-physics retroreflector

Retroreflectors are able to send all their incident energy back in the same direction from where the incident wave is coming [see Fig. 6(a)]. Following the design methodology explained above, we design a retroreflector that works for acoustic and TM-polarized electromagnetic waves. The first step in the design of the multidisciplinary retroreflector is to choose an appropriate reflector profile. In this work, for simplicity we use the simplest surface profile: a flat surface located in the *x*-*z* plane. As shown above, this is possible because the desired field structure is purely a standing wave, without any power flow across any surface.

Once the position of the retroreflecting surface is defined, the periodicity is fixed by the operation frequencies, both in acoustics, $f_{\rm ac}$, and in electromagnetism, $f_{\rm EM}$. We start from considering the simplest case when the frequencies are such that $\lambda_{\rm ac} = \lambda_{\rm EM}$, i.e., the periodicity for both electromagnetic and acoustic scenarios is the same ($D_{\rm ac} = D_{\rm EM}$). To satisfy this condition, the frequencies should be related as $f_{\rm EM} = f_{\rm ac}c_{\rm EM}/c_{\rm ac}$. As an example, we assume that the background medium is air, characterized by $c_{\rm EM} = 3\cdot 10^8$ m/s and $c_{\rm ac} = 343$ m/s (the speed of sound in the background media is calculated using a reference temperature of $T = 20°$C).

The last step in the design is to implement the required surface impedances. For flat retroreflectors, the required surface impedances for electromagnetic and acoustic waves can be written as

$$Z_s^{\rm ac}(x) = j\,\frac{Z_0^{\rm ac}}{\cos\theta_i}\cot\left(k_{\rm ac}\sin\theta_i x\right), \tag{8}$$

$$Z_s^{\rm EM}(x) = -jZ_0^{\rm EM}\cos\theta_i\tan\left(k_{\rm ac}\sin\theta_i x\right) \tag{9}$$

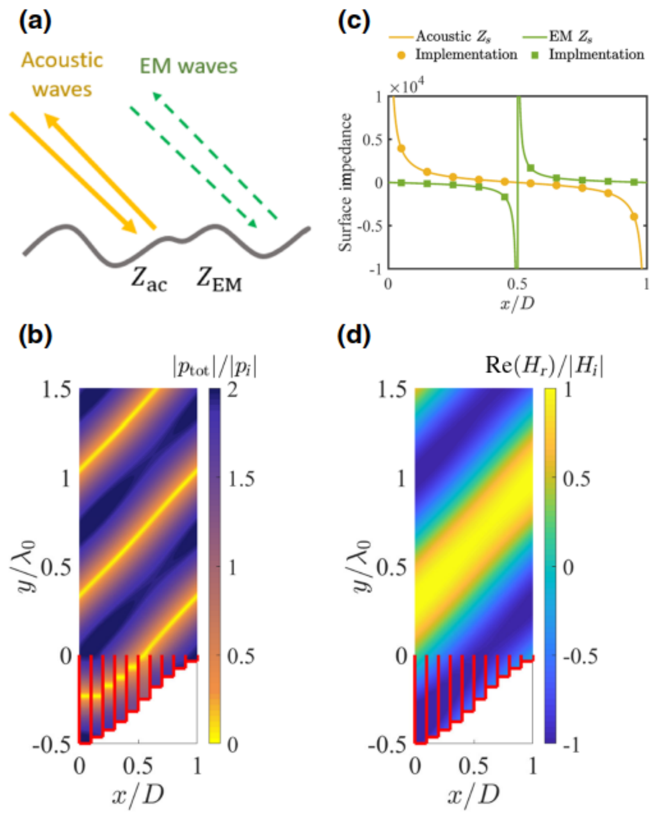

FIG. 6. The dual-physics retroreflector. (a) A schematic representation of the metasurface. (b) The total pressure field calculated using a numerical simulation for acoustic waves. The red lines denote the hard boundary conditions used for simulating the grooves. (c) The surface impedance for electromagnetic (EM) and acoustic metasurfaces. (d) The reflected magnetic field calculated using a numerical simulation for EM waves. The red lines denote the PEC boundary conditions used for simulating the grooves.

The surface-impedance values when $\theta_i = 70°$ are represented in Fig 6(c). These surface-impedance profiles can be implemented using empty closed-ended grooves as meta-atoms. The depths of the grooves are 50.0, 46.4, 42.4, 37.7, 31.9, 25.0, 18.1, 12.3, 7.60, and 3.60 mm (from left to right). Figures 6(b) and 6(d) show the results of the numerical simulation of a multidisciplinary retroreflector for $f_{\rm ac} = 3430$ Hz and $f_{\rm EM} = 3$ GHz. From the distribution of the total acoustic field represented in Fig. 6(b), we can see how a standing wave is generated as a consequence of interference between the incident and reflected waves. Figure 6(d) shows the reflected field in the electromagnetic scenario, where we can see that all the energy is sent back along the propagation axis of the incident wave.

If the acoustic and electromagnetic frequencies are arbitrary and the corresponding wavelengths are not equal, the required periodicity of the metasurface for each scenario will be different, $D_{\rm ac} \neq D_{\rm EM}$. In this case, we select the period of the structure to be equal to the least common multiple of the two periods. It is also important to note in this general case that the relation between the acoustic and electromagnetic surface impedances is not described by Eqs. (8) and (9). Thus, implementation with simple closed-ended grooves is not possible. In this case, we should use meta-atoms consisting of partially filled closed-ended grooves or closed-ended grooves with a metallic grid, which allow realizations of the required impedance profiles for both fields. Two examples on how to use these meta-atoms are given in Sec. III B.

2. Dual-physics anomalous reflector

The second example is an anomalous reflector for acoustic and electromagnetic waves. The schematic representation of the proposed metasurface is shown in Fig. 7(a). This device is able to send impinging acoustic and electromagnetic plane waves coming from a certain direction in an arbitrary direction. As explained in Sec. II, in this case there is a periodic power-flow distribution in the x-y plane. Following the design procedure for power-flow–conformal reflective metasurfaces, the first step is to define an appropriate surface profile for the desired incident angle θ_i and the desired reflection angle θ_r, ensuring that the power flow is always tangential to the reflecting surface. The second step in the design is to implement the required surface impedances for both acoustic and electromagnetic waves. In this case, we follow a similar approach as in the previous example and exploit the fact that the normalized $Z_{\rm ac}$ is analogous to normalized $Y_{\rm TM}$. As already demonstrated, using empty metallic closed-ended grooves we can realize a metasurface with the desired acoustic and electromagnetic properties. In particular, for an anomalous reflector with $\theta_i = 0^\circ$ and $\theta_r = 70^\circ$, the required depths of the grooves, from left to right, are 5.90, 7.80, 10.0, 11.7, 49.5, 38.3, 40.1, 42.2, 44.2, 46.0, 47.6, 49.2, 0.80, 2.40, and 4.10 mm (considering the frequencies $f_{\rm EM} =$ 3 GHz and $f_{\rm ac} = 3430$ Hz as an example). Figures 7(b) and 7(d) show the scattered fields produced by the structure at the operation frequency for both the acoustic and the electromagnetic scenarios.

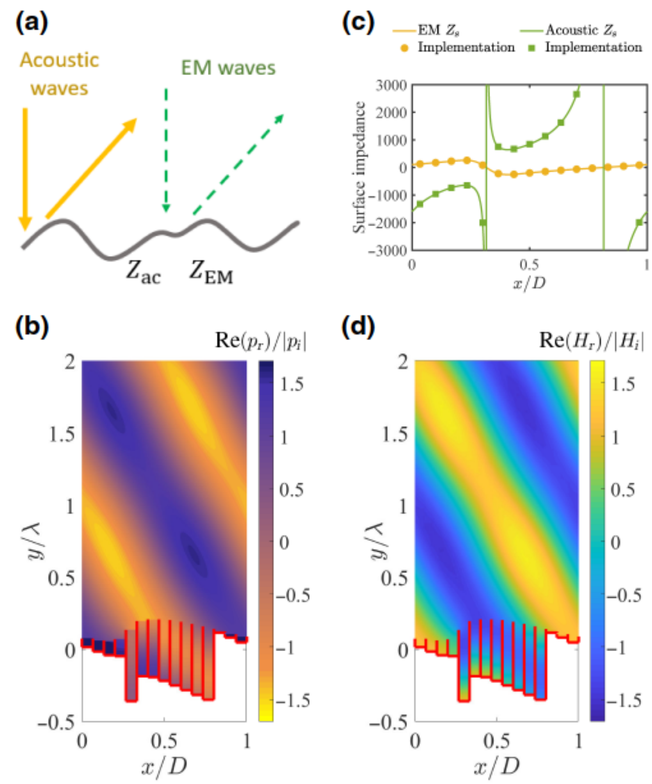

FIG. 7. The dual-physics anomalous reflector. (a) A schematic representation of the metasurface. (b) The reflected pressure field calculated using a numerical simulation for acoustic waves. The red lines denote the hard boundary conditions used for simulating the grooves. (c) The surface impedances for electromagnetic (EM) and acoustic metasurfaces. (d) The reflected magnetic field calculated using a numerical simulation for EM waves. The red lines denote the PEC boundary conditions used for simulating the groove walls.

B. Different functionalities in the same platform

The previous examples have shown the possibility of exploiting the local behavior of power-flow–conformal metasurfaces and the direct analogy between acoustic and electromagnetic waves to implement multidisciplinary metadevices that produce the same response for acoustic and electromagnetic waves. Next, we propose metadevices realizing different transformations for acoustic and electromagnetic waves. As particular examples, we study a retroreflector with different angles for acoustic and electromagnetic waves and an anomalous reflector for acoustic waves that behaves as a retroreflector for electromagnetic waves.

1. Dual-physics retroreflector for different angles

Here, we propose an implementation of flat retroreflectors able to work at different angles for acoustic and electromagnetic waves [see Fig. 8(a)]. The incident angle of electromagnetic illumination, $\theta_{\rm EM}$, determines the periodicity for electromagnetic waves $D_{\rm EM} = \lambda_{\rm EM}/2\sin\theta_{\rm EM}$. Then, we define the periodicity for acoustic waves to be m times bigger than the periodicity for electromagnetic waves $D_{\rm ac} = \lambda_{\rm ac}/2\sin\theta_{\rm ac} = mD_{\rm EM}$. The free choice of the coefficient m allows us to control the operating incident angle for acoustic waves as $\theta_{\rm ac} = \arcsin(\lambda_{\rm ac}\sin\theta_{\rm EM}/m\lambda_{\rm EM})$. In our example, we assume that $\lambda_{\rm ac} = \lambda_{\rm EM}$ by choosing the operation frequencies to be equal to $f_{\rm EM} = 3$ GHz and $f_{\rm ac} = 3430$ Hz. If we choose $m = 2$ and $\theta_{\rm EM} = 80^\circ$, then $\theta_{\rm ac} = \arcsin(\sin\theta_{\rm EM}/2) = 29.5^\circ$.

The next step in the design is to implement the required surface impedance for both the acoustic and the electromagnetic scenarios [see Fig. 8(c)]. The main difference

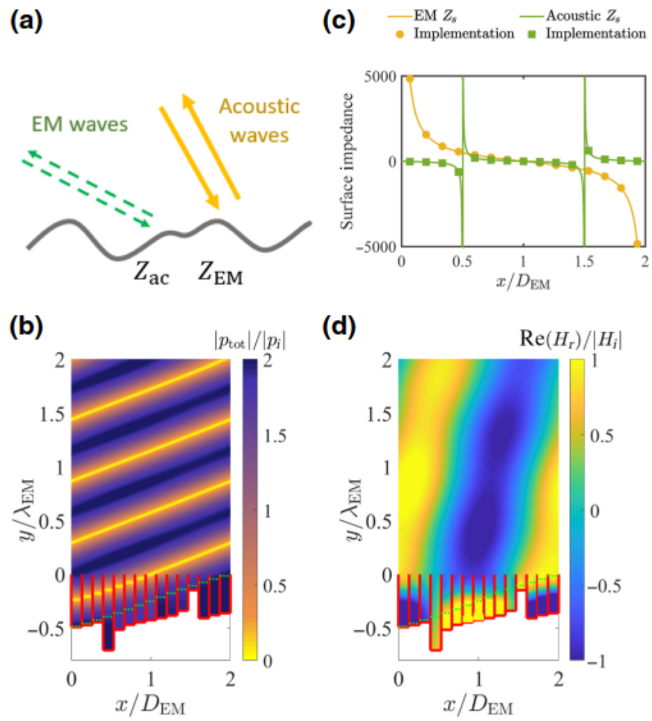

FIG. 8. The multidisciplinary retroreflector for different angles. (a) A schematic representation of the metasurface. (b) The total pressure field calculated using a numerical simulation for acoustic waves. The red lines denote the hard boundary conditions used for simulating the grooves. The green dotted lines represent the transition between the empty groove and the solid material. (c) The surface impedance for electromagnetic (EM) and acoustic metasurfaces. (d) The reflected magnetic field calculated using a numerical simulation for EM waves. The red lines denote the PEC boundary conditions used for simulating the groove walls. The green dotted lines represent the transition between an empty groove volume and the dielectric filling material.

compared to the previous examples is that in this case there is no relation between the acoustic and electromagnetic surface impedances. For this reason, we need to use meta-atoms that offer independent control of both impedances. In this example, we choose partially filled closed-ended grooves as meta-atoms. We choose a material used for filling the tube with the relative permittivity $\varepsilon_2 = 2$. To systematically design the meta-atoms, we start implementing the acoustic response according to $Z_s^{\rm ac} = -jZ_0^{\rm ac}\cot(k_{\rm ac}\ell_1)$. The depths of the empty volume of each groove, ℓ_1, equal 48.5, 45.6, 42.6, 39.4, 36.1, 32.5, 28.8, 25.0, 21.2, 17.5, 13.9, 10.6, 7.40, 4.40, and 1.50 mm. Using Eq. (7) we can calculate the required length of the dielectric filling ℓ_2. The found values of ℓ_2 are 0.60, 1.70, 2.00, 31.3, 15.4, 14.5, 15.9, 17.7, 19.5, 20.9, 20.0, 4.10, 33.4, 33.7, and 34.7 mm, respectively. The lengths of the grooves are given from left to right. In Fig. 8(c), a comparison between the required surface impedances and the impedances implemented with the actual meta-atoms is presented. Figures 8(b) and 8(d) show the results of a numerical simulation of the structure response for acoustic and electromagnetic waves, where we can see standing waves generated by the incident and reflected waves, with different operational angles for acoustic and electromagnetic waves.

2. Acoustic anomalous reflector and EM retroreflector

In this last example, we propose and study a device that acts as a retroreflector for electromagnetic waves and as an anomalous reflector for acoustic waves [see Fig. 9(a)]. Since the electromagnetic retroreflector can be implemented with any surface profile, we start the design with the definition of the tangential to the power-flow surface for the acoustic anomalous reflector. Using the theoretical approach described in Sec. II C, we find the surface profile, $y_c = f(x)$, and calculate the surface acoustic impedance $Z_s^{\rm ac}$. For an incident angle $\theta_i^{\rm ac} = 0^\circ$ and a reflected angle $\theta_r^{\rm ac} = 60^\circ$, the acoustic impedance is represented in Fig. 9(c). In this example, for the sake of simplicity, we choose the incident angle of the electromagnetic retroreflector, $\theta_i^{\rm EM}$, that corresponds to the same surface period as for the acoustic anomalous reflector, $D_{\rm ac} = D_{\rm EM}$. Choosing the operation frequencies equal to $f_{\rm EM} = 3$ GHz and $f_{\rm ac} = 3430$ Hz, the angle of incidence for the electromagnetic retroreflector is $\theta_i^{\rm EM} = 25.65^\circ$. The electromagnetic surface impedance $Z_s^{\rm EM}$ for the surface profile defined by y_c is represented in Fig. 9(c). As mentioned before, if the electromagnetic and acoustic periods are not equal, the period of the structure is chosen as their least common multiple.

Finally, once we know a suitable surface profile and the corresponding surface impedances, we design meta-atoms that implement the surface impedance for both scenarios. Because this device requires independent control of electromagnetic and acoustic impedances, we choose as meta-atoms closed-ended grooves that are partially filled with a dielectric with relative permittivity $\varepsilon_2 = 2$. Using the analytical formulas presented at the beginning of this section, the lengths of the empty portion of the grooves, ℓ_1, that produce the desired acoustic response are 5.90, 7.80, 10.0, 11.7, 49.5, 38.3, 40.1, 42.2, 44.2, 46.0, 47.6, 49.2, 0.80, 2.40, and 4.10 mm. Then, using Eq. (7), we calculate the required lengths of the dielectric filling ℓ_2. The found values of ℓ_2 are 34.2, 30.3, 26.4, 23.4, 34.0, 7.90, 5.20, 1.50, 32.8, 28.4, 23.4, 17.8, 12.3, 7.30, and 2.80 mm, respectively. As in previous examples, the lengths of the grooves are given from left to right. Figures 9(b) and 9(d) show the results of numerical simulations for acoustic and electromagnetic waves. In Fig. 9(b), the total acoustic field is represented and we can recognize the typical interference pattern generated by the incident wave and the reflected wave. Figure 9(d) shows the reflected magnetic field, where we can see that the energy is sent back in the illumination direction.

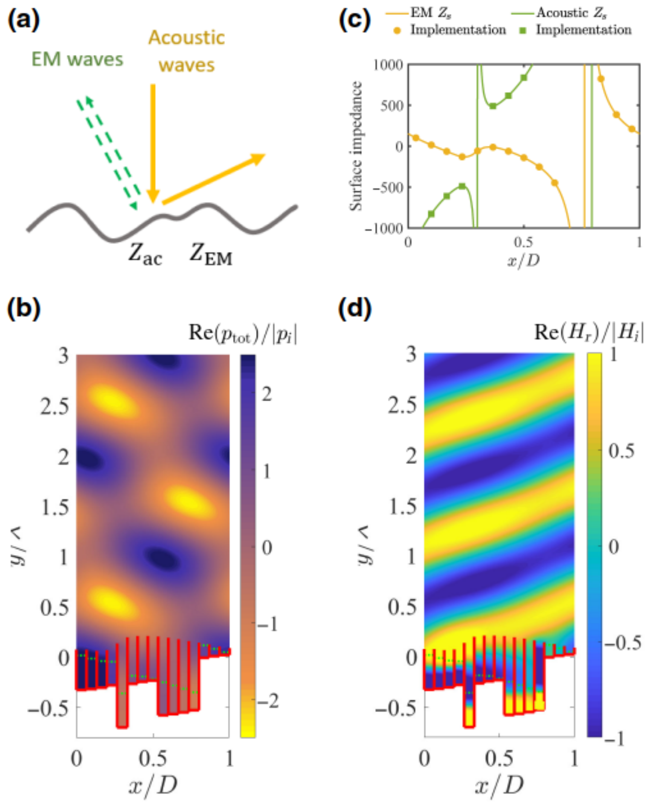

FIG. 9. The acoustic anomalous reflector and the electromagnetic retroreflector. (a) A schematic representation of the metasurface. (b) The total pressure field calculated using a numerical simulation for acoustic waves. The red lines show the hard boundary conditions used for simulating the grooves. The green dotted lines indicate the transition between the empty groove volume and the solid filling material. (c) The surface impedance for electromagnetic (EM) and acoustic metasurfaces. (d) The reflected magnetic field calculated using a numerical simulation for EM waves. The red lines denote the PEC boundaries used for simulating the groove walls. The green dotted lines represent the transition between the empty groove volume and the dielectric filling material.

IV. CONCLUSIONS

A multidisciplinary analysis of power-flow–conformal metasurfaces is performed from both acoustic and electromagnetic points of view. Based on the revealed analogy, we find the possibility of creating metasurfaces that operate as various reflectors for both electromagnetic and acoustic waves at the same tine. We propose three simple meta-atom topologies that allow us to engineer and control the electromagnetic and the acoustic responses at will. The considered example functionalities include highly efficient (theoretically perfect) retroreflection and anomalous reflection for both waves. Due to the analytical formulation, the design process is straightforward and numerical optimizations are not required. The illustrative examples presented in this work can be extended to more complex scenarios that include manipulation of multiple waves (for example, beam splitters for waves of one nature and retroreflectors for waves of the other nature) or three-dimensional transformations that require us to define the surface profile considering the variations along the z axis. If the mathematical intricacy of the problem does not allow a closed-form expression for the surface profiles to be obtained, numerical methods can be used to find the surface tangential to the power flow. This multidisciplinary approach opens up a path for the design of devices that integrate functionalities for both waves. We note that the proposed topology of dual-physics meta-atoms allows electrical tunability, for example, using switches to control metal wire grids or by using tunable materials as the filling for the grooves or tubes.

In real life, electromagnetic and acoustic waves coexist and, from a practical perspective, need to be controlled, isolated, or absorbed. For this reason, it is important to develop dual-physics systems that allow simultaneous manipulation of both waves. In addition, due to their thin profile, these devices can be integrated, for example, in domestic environments (tables, work desks, walls, etc.) or in smart cities (manipulating energy from traffic or environmental noise and electromagnetic signals used for communication purposes). We hope that our results will promote the design of compact devices capable of simultaneously controlling waves of different natures.

ACKNOWLEDGMENT

This work received funding from the Academy of Finland, Project 309421.

[1] B. Assouar, B. Liang, Y. Wu, Y. Li, J.-C. Cheng, and Y. Jing, Acoustic metasurfaces, Nat. Rev. Mater. **3**, 460 (2018).

[2] S. Glybovski, S. Tretyakov, P. Belov, Y. Kivshar, and C. Simovski, Metasurfaces: From microwaves to visible, Phys. Rep. **634**, 1 (2016).

[3] O. Quevedo-Teruel, Roadmap on metasurfaces, J. Opt. **21**, 073002 (2019).

[4] N. Estakhri and A. Alu, Wave-Front Transformation with Gradient Metasurfaces, Phys. Rev. X **6**, 041008 (2016).

[5] A. Díaz-Rubio, V. Asadchy, A. Elsakka, and S. Tretyakov, From the generalized reflection law to the realization of perfect anomalous reflectors, Sci. Adv. **3**, e1602714 (2017).

[6] A. Epstein and O. Rabinovich, Unveiling the Properties of Metagratings via a Detailed Analytical Model for Synthesis and Analysis, Phys. Rev. Appl. **8**, 054037 (2017).

[7] Y. Ra'di, D. L. Sounas, and A. Alu, Metagratings: Beyond the Limits of Graded Metasurfaces for Wave Front Control, Phys. Rev. Lett. **119**, 067404 (2018).

[8] D. Kwon, Lossless scalar metasurfaces for anomalous reflection based on efficient surface field optimization, IEEE Antennas Wirel. Propag. Lett. **17**, 1149 (2018).

[9] V. Asadchy, A. Díaz-Rubio, S. Tcvetkova, D. Kwon, A. Elsakka, M. Albooyeh, and S. Tretyakov, Flat Engineered Multichannel Reflectors, Phys. Rev. X **7**, 031046 (2017).

[10] A. Díaz-Rubio and S. Tretyakov, Acoustic metasurfaces for scattering-free anomalous reflection and refraction, Phys. Rev. B **96**, 125409 (2017).

[11] D. Torrent, Acoustic anomalous reflectors based on diffraction grating engineering, Phys. Rev. B **98**, 060101(R) (2018).

[12] A. Díaz-Rubio, J. Li, C. Shen, S. Cummer, and S. Tretyakov, Power flow conformal metamirrors for engineering wave reflections, Sci. Adv. **5**, eaau7288 (2019).

[13] C. Shen, A. Díaz-Rubio, J. Li, and S. Cummer, A surface impedance-based three-channel acoustic metasurface retroreflector, Appl. Phys. Lett. **112**, 183503 (2018).

[14] V. Popov, F. Boust, and S. N. Burokur, Controlling Diffraction Patterns with Metagratings, Phys. Rev. Appl. **101**, 011002 (2018).

[15] J. Carbonell, D. Torrent, A. Díaz-Rubio, and J. Sánchez-Dehesa, Multidisciplinary approach to cylindrical anisotropic metamaterials, New J. Phys. **13**, 103034 (2011).

[16] L. Felsen and N. Marcuvitz, *Radiation and Scattering of Waves* (Wiley-IEEE Press, New York, 1994).

[17] L. Brekhovskikh, *Waves in Layered Media* (Academic Press, London, 1976).

[18] S. Tretyakov, *Analytical Modeling in Applied Electromagnetics* (Artech House, Norwood, MA, 2003).